Experimental Neurology 236 (2012) 171–178

Contents lists available at SciVerse ScienceDirect

Experimental Neurology

journal homepage: www.elsevier.com/locate/yexnr

Disruption of Purkinje cell function prior to huntingtin accumulation and cell loss in an animal model of Huntington Disease

S.E. Dougherty [a,d], J.L. Reeves [b], E.K. Lucas [c], K.L. Gamble [d], M. Lesort [d], R.M. Cowell [d,*]

[a] Neuroscience Graduate Program, University of Alabama at Birmingham, USA
[b] Neuroscience Undergraduate Program, University of Alabama at Birmingham, USA
[c] Department of Psychiatry, Weill Cornell Medical College, USA
[d] Department of Psychiatry & Behavioral Neurobiology, University of Alabama at Birmingham, USA

ARTICLE INFO

Article history:
Received 2 March 2012
Revised 17 April 2012
Accepted 23 April 2012
Available online 2 May 2012

Keywords:
Cerebellum
Gene expression
Motor impairment
Stereology
Glutamic acid decarboxylase 67
Calbindin
Parvalbumin
Loose patch electrophysiology

ABSTRACT

Huntington Disease (HD) is a devastating neurological disorder characterized by progressive deterioration of psychiatric, motor, and cognitive function. Purkinje cells (PCs), the output neurons of the cerebellar cortex, have been found to be vulnerable in multiple CAG repeat disorders, but little is known about the involvement of PC dysfunction in HD. To investigate possible PC abnormalities, we performed quantitative real time PCR, Western blot analysis, and immunohistochemistry experiments to explore the changes in PC markers in the R6/2 mouse model of severe HD. There were reductions in the transcript and protein levels of the calcium-binding proteins parvalbumin and calbindin, as well as the enzyme glutamic acid decarboxylase 67. Immunohistochemistry supported these results, with the most substantial changes occurring in the PC layer. To determine whether the reductions in PC marker expression were due to cell loss, we performed stereology on both presymptomatic and end-stage R6/2 mice. Stereological counts indicated a significant reduction in PC number by end-stage but no change in presymptomatic animals (4 weeks of age). To assess cellular function prior to cell loss and symptom onset, we measured spontaneous firing in PCs from 4-week old animals and found a striking deficit in PC firing as indicated by a 57% decrease in spike rate. Interestingly, huntingtin inclusions were not widely observed in PCs until 12 weeks of age, indicating that soluble huntingtin and/or abnormalities in other cell types may contribute to PC dysfunction. Considering the roles for PCs in motor control, these data suggest that early PC dysfunction potentially contributes to motor impairment in this model of HD.

Introduction

Huntington Disease (HD) is an autosomal dominant neurodegenerative disorder characterized by progressive deterioration of cognitive, motor, and psychiatric function. HD is caused by an elongation of the CAG repeat in exon 1 of the huntingtin gene, with an inverse correlation between age of onset and repeat length (Group, H. s. D. C. R., 1993). Expression of mutant huntingtin (mthtt) is ubiquitous throughout the brain and is thought to be involved in a number of pathological interactions. These functions include transcriptional dysregulation (Bithell et al., 2009; Cha et al., 1998; Hodges et al., 2006; Imarisio et al., 2008; Luthi-Carter et al., 2002; Strand et al., 2005), interruption of calcium signaling (Giacomello et al., 2011; Perry et al., 2010), and disruption of normal synaptic physiology (Cummings et al., 2009; Klapstein et al., 2001; Milnerwood and Raymond, 2007; Morton et al., 2001).

While the striatum is the primarily affected brain region in HD, it is possible that other components of the motor circuit, such as the cerebellum, are involved in motor symptom development. Conflicting reports have been made on the pathology of the cerebellum in HD which range from the region being considered unaffected (Carroll et al., 2011; Van Raamsdonk et al., 2007) to the cerebellum being an important part of the disease progression (Fennema-Notestine et al., 2004; Rodda, 1981; Rosas et al., 2003; Ruocco et al., 2006a, 2006b). The cerebellum appears to be more commonly affected in juvenile HD as exhibited by a loss in overall cerebellar volume (Fennema-Notestine et al., 2004; Kageyama et al., 2003; Nicolas et al., 2011; Ruocco et al., 2006a, 2006b; Sakazume et al., 2009). It is imperative to explore cerebellar pathology in animal models of HD to determine the involvement of this brain region in the pathogenesis of HD.

The output neurons of the cerebellar cortex are the GABAergic Purkinje cells (PCs). Intranuclear inclusions have been found in PCs in postmortem tissue from HD patients and in knock-in animal models of HD (Adachi et al., 2001). Additionally PCs are vulnerable in both patient and animal models of other CAG repeat disorders (Garden et al.,

* Corresponding author at: Department of Psychiatry & Behavioral Neurobiology, 728 Sparks Building, 1720 7th Avenue South, Birmingham, AL 35294, USA. Fax: +1 205 975 4879.
E-mail address: rcowell@uab.edu (RM. Cowell).

0014-4886/$ – see front matter © 2012 Elsevier Inc. All rights reserved.
doi:10.1016/j.expneurol.2012.04.015

2002; Koeppen, 1991, 2005; Schulz et al., 2010; Vig et al., 1996, 1998). Investigators have often considered the cerebellum to be unaffected in HD and used the cerebellum as a control region. Nonetheless, there is evidence to suggest a reduced density of PCs in HD patients (Fennema-Notestine et al., 2004; Jeste et al., 1984; Rosas et al., 2003) raising the possibility that PCs play a meaningful role in HD.

Little is known about PC function or survival in animal models of HD. To investigate the involvement of PC dysfunction in HD, we utilized the R6/2 model. The R6/2 mouse model of HD carries transgenic expression of exon 1 of the human huntingtin gene with an expanded CAG repeat (Mangiarini et al., 1996). This model has been shown to be a severe model of HD with an abbreviated lifespan, early symptom onset and enhanced disease severity. This increased severity might suggest a more global neurological assault (Ruocco et al., 2008); as such, it follows that investigation of cerebellar changes in the R6/2 mouse could provide insights into the involvement of this brain region in early onset HD.

In these experiments we explored the changes that occur in PCs of R6/2 mice using qRT-PCR, immunohistochemical staining, and electrophysiology. Here we report decreases in GABAergic cell markers and calcium binding proteins in the cerebellum, specifically the PC layer. These changes were accompanied by huntingtin accumulation and PC loss in symptomatic mice but preceded by alterations in cellular physiology. These studies suggest that PCs are vulnerable in R6/2 mice and may contribute to the development of motor symptoms in HD.

Methods

Animals

The Institutional Animal Care and Use Committee of the University of Alabama at Birmingham approved all experimental protocols. The R6/2 mouse line was obtained from Jackson Laboratories and maintained through breeding male F1 generation offspring to WT hybrid (B6CBA) females (B6CBA-Tg(HDexon1)62Gpb/3J). The mice were obtained from Jackson Laboratories by way of an ovarian transplant female with ovaries from a sexually unviable R6/2 +/− female. All experiments were conducted with both male and female animals at ages 2, 4, 7, and 12 weeks. R6/2 mice carried a repeat length of 167 as genotyped by Laragen, Inc (Culver City, CA). These animals were housed in groups of up to 5 animals per cage with food and water ad libitum.

Behavioral assessment

Behavioral analyses were conducted on littermates at four, six or twelve weeks of age during the lights on period (6 am–6 pm). All experiments were conducted blind to the genotype of the animals.

Rotarod

The rotarod apparatus (MedAssociates, St. Albins, VT) consisted of a 5-station treadmill with a computer-controlled stepper motor-driven rod with constant speed or accelerating speed modes of operation. Animals were trained on the rotarod for four days. On the first day of the training period, animals were placed on the treadmill at an accelerating speed of 2–24 rotations per minute (rpm) for a maximum of 60 s for a total of 5 trials. On the second through fourth days, the animals were placed on the treadmill at a constant speed of 16 rpm for a maximum of 60 s for a total of 5 trials per day. On the fifth day, animals underwent two trials each at rotating speeds 16, 20, 24, 28, and 32 fixed rpm. Each trial lasted for a maximum of 60 s, during which latencies to fall were recorded. Mice were allowed to rest for at least 5 min between each trial.

Open field

Animals were placed in a square apparatus (27.9 cm^2) consisting of 48 infrared beams (MedAssociates) for 30 min. Data were collected with Open Field Activity Software (MedAssociates) in 1 minute intervals over the test period, and total ambulatory time and distance were determined.

Gene expression analysis

Protocols were performed as described (Lucas et al., 2010). Briefly, mice were anesthetized with isoflourane and sacrificed by decapitation. Brains were removed, and dissected by anatomical region. Tissues were flash frozen on dry ice and kept in the −80 °C freezer until use. At least 12 h prior to processing, tissues were placed in RNA*later*-ICE (Ambion Austin, TX) cooled to −80 °C and then kept at −20 °C until homogenization. Homogenization was performed with a Tissue-Tearor (Biospec Bartlesville, OK) homogenizer in Trizol following the manufacturer's instructions (Invitrogen Grand Island, NY). Taqman PCR was conducted with JumpStart Taq Readymix (Sigma St. Louis, MO) and Applied Biosystems (Carlsbad, California) primers for GAD67 (Mm00725661_s1), calbindin (Mm00486645_m1), parvalbumin (Mm00443100_m1), and β-actin (Mm00607939_s1).

Immunofluorescence

Animals were anesthetized with isofluorane and perfused intracardially with room temperature 4% paraformaldehyde in phosphate buffered saline (PBS). Brains were removed and postfixed for an additional 24–72 h. The samples were cryoprotected in graded sucrose over a 5 day period and then embedded and frozen in a mixture of 20% sucrose and Tissue-Tek O.C.T. Compound (Sakura Finetek USA, Inc. Torrance, CA) and stored at −80 °C. Tissue blocks were sectioned at 30 μm, mounted onto charged slides (Fisher) and allowed to dry overnight before storage at −80 °C. Slides were then thawed and washed with PBS followed by a 1 h incubation in 10% serum (from the host of the 2° antibody) and PBS with 3% bovine serum albumin (BSA). The slides were then incubated overnight with a predetermined concentration of 1° antibody and 5% serum in 0.3% Triton X PBS with 3% BSA. This is followed by washing and then a 2 h incubation with the corresponding fluorescence-conjugated 2° antibody (Jackson ImmunoResearch West Grove, PA) and 5% serum in 0.3% Triton X PBS with 3% BSA. The slides are then immediately mounted using an antifade media containing DAPI, coverslipped and left to dry at room temperature overnight. When necessary, a Vector (Burlingame, CA) Mouse on Mouse Kit (Fluorescein Cat No. FMK-2201) was used to minimize background staining for mouse-made antibodies.

Western blot analysis

Cerebella were homogenized in RIPA buffer (150 mM NaCl, 50 mM Tris, 1% Triton X-100, 1% sodium dodecyl sulfate, 0.5% deoxycholic acid; pH 8.0) containing a protease inhibitor tablet (Complete Mini, Roche Diagnostics Indianapolis, IN). Total protein concentration was determined with a bicinchonicic acid protein assay kit (Thermo Scientific Waltham, MA), and absorbance was measured at 540 nm. Protein was denatured in sample buffer (62.5 mM Tris–HCl, 20% glycerol, 2% sodium dodecyl sulfate, 5% β-mercaptoethanol; pH 6.8) at 95 °C. Equivalent amounts of protein were loaded into precast polyacrylamide NuPage gels (Invitrogen). One interblot control sample was loaded onto every gel to permit comparison among gels. Protein was transferred onto nitrocellulose membranes. Blots were blocked with 5% milk in Tris buffered saline (TBS; pH 7.6) with 1% Tween (TBS-T) and probed with primary antibodies in 5% IgG-free BSA (Jackson ImmunoResearch) TBS-T overnight at 4 °C and peroxidase-conjugated secondary antibodies (Jackson ImmunoResearch) in 5% milk TBS-T for 1 h at room temperature.

Blots were incubated in chemiluminescent substrate (Thermo Scientific Pittsburg, PA) and exposed to film. The optical density of bands was calculated after background subtraction using UN-SCAN-IT gel analysis software (Silk Scientific Inc. Orem, UT). All bands were normalized to the interblot control band, then to actin and expressed as mean optical density mean ± SEM.

Antibody information

Immunostaining was performed with antibodies specific to the following proteins: mouse monoclonal GAD67 (MAB5406, Millipore Billerica, MA) at a dilution of 1:500 for fluorescence, 1:1000 for Western; mouse monoclonal Calb (C9848, Sigma) at a dilution of 1:2000 for fluorescence, 1:5000 for Western; rabbit polyclonal PV (PV25, Swant) at a dilution of 1:500 for fluorescence; mouse monoclonal PV (Millipore) at a dilution of 1:500 for Western; and goat polyclonal Huntingtin (SC-8767, Santa Cruz) at a dilution of 1:100 for fluorescence.

Stereology

Animals were anesthetized with isofluorane and perfused intracardially with room temperature 4% paraformaldehyde in phosphate buffered saline (PBS). Brains were removed and postfixed for an additional 24–72 h. The samples were cryoprotected in graded sucrose over a 5 day period and then embedded and frozen in a mixture of 20% sucrose and Tissue-Tek O.C.T. Compound (Sakura Finetek USA, Inc. Torrance, CA) and stored at −80 °C. Tissue blocks were sectioned at 30 μm, mounted onto charged slides (Fisher) and allowed to dry overnight before storage at −80 °C. Slides were then thawed and washed with distilled H_2O for 5 min followed by a 10 minute incubation in hematoxylin (Sigma). Slides were incubated in running H_2O for 15 min followed by a 1 minute incubation in eosin (Sigma). Slides were then dehydrated and cover-slipped using Permount (Fisher).

Cells were counted by an unbiased investigator blinded to animal genotype using StereoInvestigator (MicroBrightField, Inc Williston, VT). Pilot animals were used to determine parameters needed to give optimal counting precision. The optical fractionator method was used to generate an estimate of PCs counted in an unbiased selection of serial sections in a defined volume of the cerebellum. Serially cut 30 μm thick sagittal tissue sections (every twentieth section) were analyzed throughout the entire cerebellum of animals in each cohort (n = 3/genotype). The number of PCs within the entire cerebellum was quantified using the optical fractionator method with dissectors placed randomly according to a 263.68 × 212.13 μm grid. The counting frame was 60 × 60 μm and the dissector height was 26 μm. On average, 150 sites were counted per section. An estimation of cell population number was provided using overall raw counts and mean section thickness.

Cell attached loose patch recording

Mice (4 week old) were anesthetized with isoflourane and sacrificed by decapitation. Brains were placed in ice-cold artificial CSF (ACSF) containing the following (in mM): 125 NaCl, 2.5 KCl, 2 $CaCl_2$, 1 $MgCl_2$, 25 $NaHCO_3$ 1.25 Na_2HPO_4 and 25 D-glucose with a pH of 7.4 and osmolality of 295 ± 5 mOsm. The ringer solution was bubbled with 95% O_2/5% CO_2. Sagittal cerebellar slices (300 μm thick) were cut using a Vibratome (7000 smz, Campden Instruments: Sarasota, FL). The slices were allowed to rest for 60 min at room temperature (22–23 °C); all experiments were then performed at room temperature. Slices were superfused continuously with oxygenated recording ACSF at room temperature. Slices were viewed with an upright microscope (Zeiss Axio Examiner A1) using infrared-differential interference contrast optics. Loose patch recordings were acquired from visually identified PC using Axio Vision 4.8 software. Cellular activity was recorded using internal solution containing the following (in mM) 140 K-gluconate, 1 EGTA, 10 HEPES and 5 KCL, and pH 7.3. Pipette tip resistance was 2–5 MΩ. The extracellular recording pipettes, containing the internal solution, were placed under visual control directly adjacent to the soma of the cell of interest. Positive pressure was applied throughout this process followed by a brief release of pressure to form a seal averaging approximately 45 MΩ. Cell-attached, loose patch-clamp recordings were obtained using an Axon CNS Molecular Devices amplifier (Multiclamp 700B), filtered at 10 kHz and digitized at 20 kHz (Digidata 1440A). A 2 min gap-free protocol on Clampex 10.2 software was used for data collection. Detection and analysis of event frequency and inter-event interval were performed semi-automatically using the program Clampfit 10.2. The detection threshold was set for analysis based on the event amplitude from a given cell.

Data analyses

Data analyses for qRT-PCR, Western blot assays and loose patch electrophysiology were performed using Microsoft Excel. A two-tailed Student t-test assuming unequal variance was utilized to assess statistical significance. Values were considered statistically significant when the p value was less than 0.05. For the measurements of transcripts at different stages of the disease, R6/2 values were normalized to WT values at each independent age, so t-tests were used; thus, the asterisks ($p<0.05$) indicate when R6/2 values were significantly different from values for WTs of the same age.

For the open field behavior data, a two-way ANOVA (Age × Genotype) was performed using PASW 18.0. For post hoc analysis Fisher's least significant difference (LSD) procedure was utilized. Values were considered statistically significant when the p value was less than 0.05.

For the rotarod behavior data, analyses were performed using PASW 18.0. The raw time values measuring latency to fall were binned according to 33rd percentiles (i.e., 0–12.99, 13.00–59.00, and 59.01–60 s) for the maximum speed trial (32 rpm). A G-likelihood test was performed on the binned data (binned proportions were considered statistically significant when the p values were less than 0.05).

For the stereological data, a two-way ANOVA (Age × Genotype) was performed using PASW 18.0. For post hoc analysis Duncan's multiple comparison procedure was utilized. Values were considered statistically significant when the p value was less than 0.05.

Results

R6/2 mice exhibit an overt motor phenotype at midlife

In order to validate previous reports of the onset and progression of motor symptoms in the R6/2 mouse, we utilized the open field and rotarod behavior paradigms. The open field analysis revealed a hypoactive phenotype which continues throughout the lifespan of these animals (n = 8/group) (Fig. 1A). A two-way ANOVA revealed significant main effects of genotype and age ($F(1,36) = 16.1$ and $F(2,36) = 11.2$, respectively; $p<0.01$ for both) but no interaction ($F(2,36) = 2.1$, $p = 0.14$). The rotarod paradigm, which more directly tests balance and motor coordination, revealed coordination dysfunction at 32 rpm at twelve weeks of age (n = 8/group; $\chi^2(2) = 15.02$ $p<0.01$) (Fig. 1B). Additionally, there were significant differences between WT and R6/2 in the proportion of animals that fell at speeds of 28, 24, and 20 rpm, $\chi^2(2) = 22.18$, 22.18, and 8.00, respectively ($p<0.05$ for all). There was no difference between WT and R6/2 at 16 rpm at 12 weeks of age ($\chi^2(2) = 2.86$, $p = 0.24$). There were no differences between the two groups at six weeks of age (data not shown) in concordance with previously published data (Mangiarini et al., 1996).

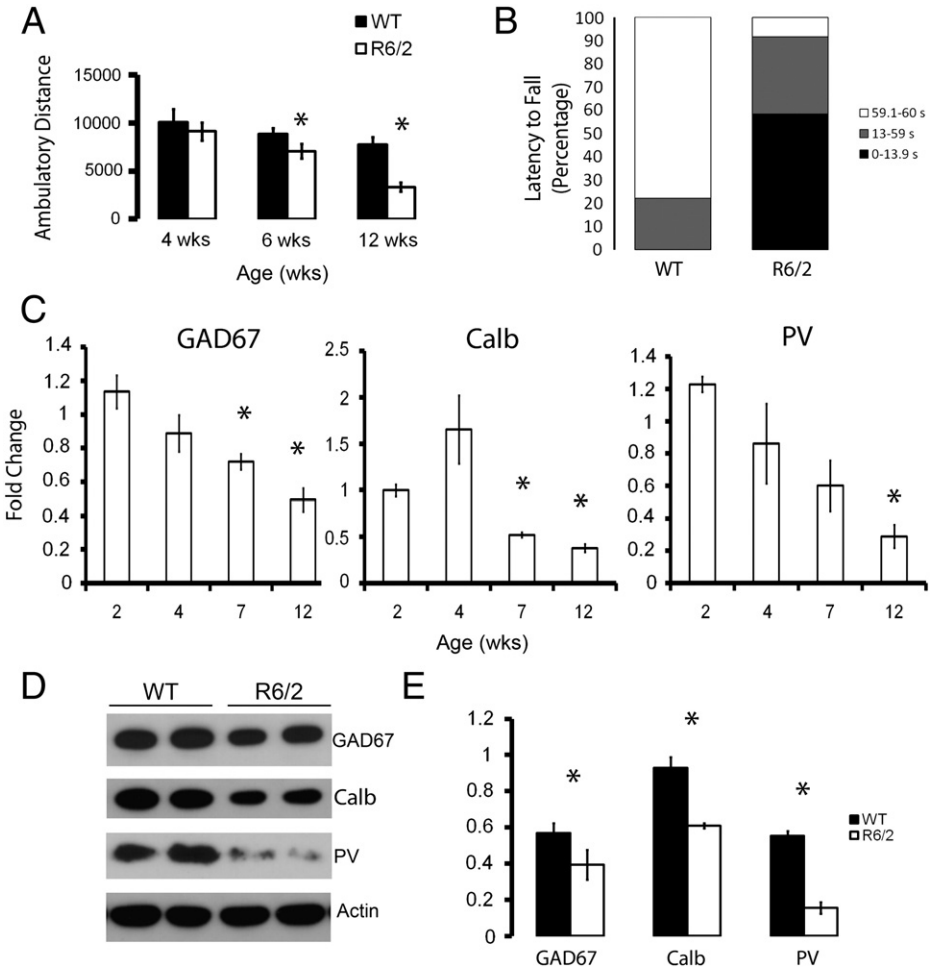

Fig. 1. R6/2 mice exhibit reductions in Purkinje cell (PC) marker expression around the age of motor symptom onset. Motor impairments were evident by reduced ambulatory distance in the open field paradigm (A) and a deficit in rotarod performance at 32 rpm at 12 weeks of age. Rotarod data is shown as percentage of animals per bin with the highest bin (59.1–60) indicative of the most successful run of a full 60 s (B). Significant deficits were also seen at 20, 24, and 28 rpm speeds while no difference was observed between groups at 6 weeks of age (data not shown). C. Using q-RT-PCR to measure transcript levels on cerebellar homogenates, expression of Purkinje markers was reduced in R6/2 mice, with GAD67 and Calb reduced by 7 weeks and PV reduced by 12 weeks (n = 9/group at 7 and 12 weeks, n = 5/group at 2 and 4 weeks). Values for mRNA levels were normalized to actin and then compared to WT (fold = 1). D. Western blot analysis revealed a decrease in protein level of GAD67, Calb and PV at 12 weeks of age (n = 7 per/group). E. Quantification of Western blot. Two-way ANOVA tests were performed on the behavioral data. Two-tailed Student's t-tests were performed on transcription and Western blot data with significance established as compared to age-matched WT. Error bars: SEM. (*$p<0.05$).

GABAergic cell markers are decreased in the cerebellum of R6/2 mice around the time of motor onset

To initially determine whether alterations in PCs occur in the R6/2 model, we performed qRT-PCR to evaluate the levels of transcripts that are highly concentrated in PCs. Transcript levels were normalized to the internal control gene, actin, and then reported as fold WT (WT = 1.0). There were no changes in actin between R6/2 and WT mice at any age. There was a decrease in the level of GAD67 ($p<0.05$) and Calb ($p<0.05$) transcript at seven and twelve weeks of age (n = 9/group, compared to age-matched WT littermates) and a reduction in PV transcript ($p<0.05$) by twelve weeks of age (Fig. 1C; n = 9/group). Student's t tests were utilized to assess alterations at individual ages since R6/2 values were only compared to values from WT mice of the same age. We then evaluated these changes in expression at the protein level in cerebellum homogenates; protein analysis revealed significant decreases in GAD67, PV, and Calb by twelve weeks of age in the R6/2 mice as compared to WT littermates (n = 7/group, two-tailed Student's t test, $p<0.05$; Figs. 1D and E). To localize the protein changes to specific cell types, immunohistochemistry was performed; immunoreactivity for GAD67 (Figs. 2C and D), Calb (Figs. 2G and H) and PV (Figs. 2K and L) was reduced markedly in the PC layer of R6/2 cerebellum. Strikingly, the interneurons of the molecular layer retained their basal levels of PV (Fig. 2L, arrows). These staining patterns suggest alterations specifically in the PCs within the cerebellum of the R6/2 mice. At four weeks of age, there is no reduction in GAD67, Calb, or PV immunostaining in the R6/2 as compared to WT (Figs. 2A and B, E and F and I and J, respectively).

R6/2 mice exhibit a loss of Purkinje cells by end stage

One explanation for the loss of PC markers could be a reduction in the total cell number in the R6/2 mice. In order to investigate whether decreases in protein and transcript levels stem from localized molecular loss within intact cells or from a loss of PC bodies, we performed stereological investigation on R6/2 mice and WT littermates. Stereological counts revealed no significant decrease in PC number at four weeks of age in the R6/2 mice (Figs. 3A and B). A population estimate using mean section thickness gave an estimate of an average of 84,886 cells in 4 week WT and 107,961 cells in 4 week R6/2 animals. There is a 55% reduction in PC number at twelve weeks of age, as compared to WT littermates (Figs. 3C and D). A population estimate using mean section thickness gave an estimate of an average of 97,208 cells in 12-week WT and 43,667 cells in 12-week R6/2 animals. A two-way ANOVA revealed no significant main effects of age or genotype, $F(1,8) = 1.57$ ($p = 0.25$) and $F(1,8) = 4.57$ ($p = 0.07$),

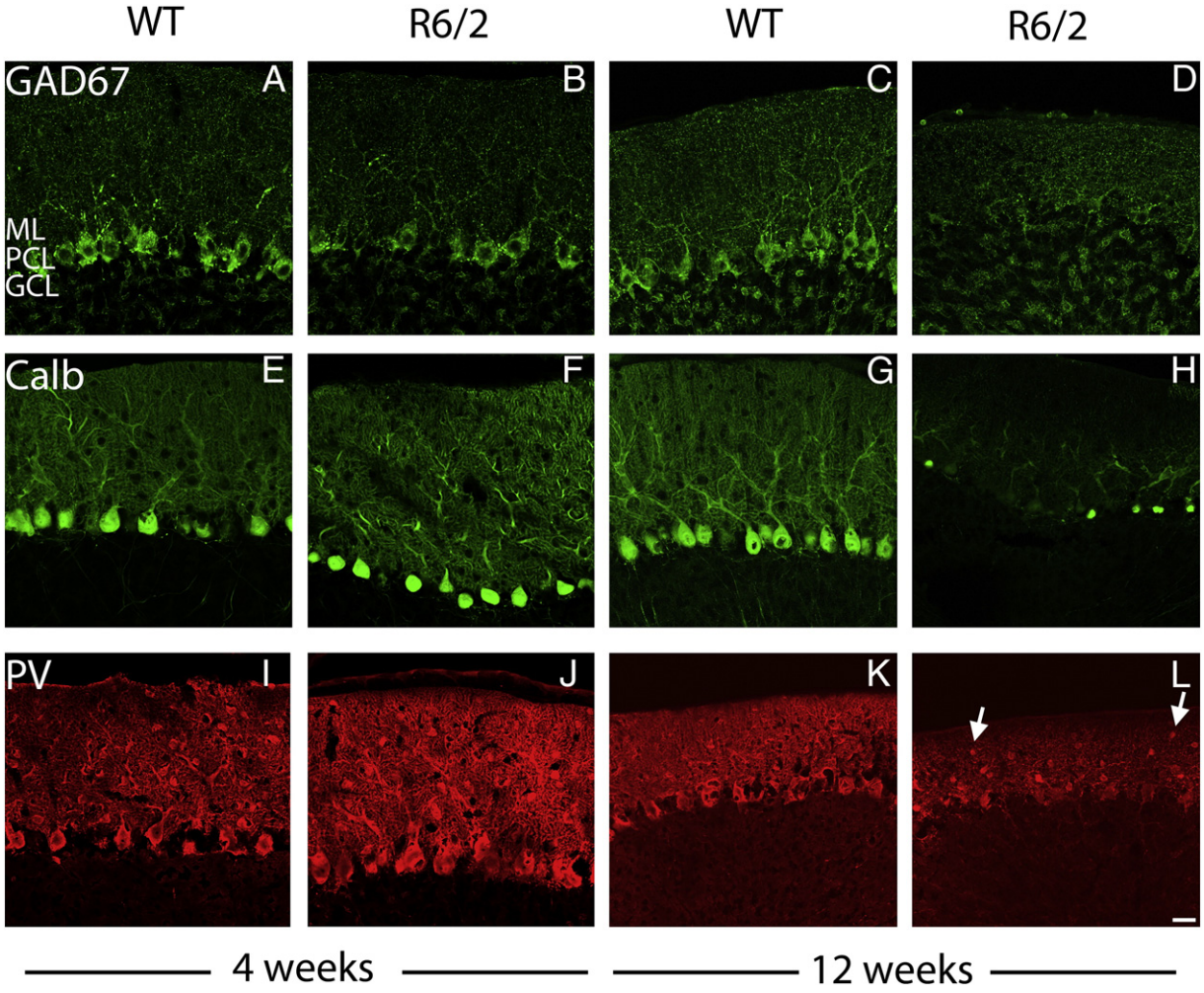

Fig. 2. Immunoreactivity for GAD67, calbindin (Calb) and parvalbumin (PV) is reduced in the Purkinje cell (PC) layer of the cerebellum at 12 weeks of age but unaltered at 4 weeks of age. A–D. Immunofluorescence with an antibody specific for GAD67 reveals a loss of staining in the PC layer of 12 week old R6/2 animals (D) as compared to 12 week old WT (C). There is no difference between groups at 4 weeks of age (A and B). E–H. An antibody specific for Calb shows a decrease in protein levels throughout the molecular and PC layers of 12-week-old R6/2 animals as compared to WT (H). There is no difference between groups at 4 weeks of age (E and F). I–L. Changes, similar to those seen in GAD67, are seen with an antibody specific to PV. Staining shows a decrease in protein levels in the PC layer of 12-week-old R6/2 animals as compared to WT (L). Staining is clearly retained in the interneurons of the molecular layer (arrows in L). ML: molecular layer. PCL: PC layer. GCL: granule cell layer. Scale bar, 25 μm.

respectively. However, there was a significant Age × Genotype interaction, $F(1,8) = 9.92$, $p < 0.05$ ($n = 3$ animals/group). Duncan's multiple comparison procedure showed that the R6/2 12-week old animals had a mean cell count that was significantly reduced from the other three group's mean cell counts. The lack of a difference in cell number between WT and R6/2 mice at 4 weeks of age suggests that the production and migration of these cells is not affected during development.

Purkinje cells exhibit a reduction in firing rate prior to motor symptom onset and transcriptional changes in R6/2 mice

The motor abnormalities observed in the R6/2 mouse model of HD arise prior to an overt loss of PCs in the cerebellum. In order to elucidate the possible role of early alterations in cellular function in this cell population, cell-attached loose-patch recordings were performed in presymptomatic animals (4 weeks of age). Using an acute slice preparation, overall spike rate was recorded from 4-week-old R6/2 mice and WT littermates. Slices were incubated in ACSF and, once patched, allowed to acclimate to the pipette tip for 3 min in order to eliminate any events in response to mechanical stimulation. Spontaneous events were then recorded for 3 min with no stimulation. Cells with fewer than five spikes within the recording interval were excluded. Loose patch recordings revealed a significant reduction in the spike frequency in the R6/2 mice as compared to WT littermates at four weeks of age, prior to the onset of motor symptoms ($n = 4$ for R6/2 and $n = 5$ for WT with 15 and 17 cells, respectively; two-tailed Student t test, $p < 0.05$; Figs. 4A and B).

Intranuclear inclusions are not evident in Purkinje cells at the time of electrophysiological deficits

To investigate the pathogenic mechanisms behind the change in firing rate, we questioned whether huntingtin inclusions were present within PCs at the time of electrophysiological deficits. Immunofluorescence using a mthtt-specific antibody revealed the presence of mthtt within the molecular and granule cell layers of the R6/2 cerebellum (Fig. 5B arrows) while staining was entirely absent in 12-week-old WT (Fig. 5A). Colocalization of mthtt-positive inclusions with PV (green, Fig. 5B, inset) in the molecular layer of 4-week-old R6/2 mice indicated that molecular layer inclusions were concentrated in molecule layer interneurons. Intriguingly, similar staining patterns were observed at 7 weeks of age, though there were more pronounced inclusions in the interneurons (enlarged in Fig. 5E) with few inclusions noted in PCs (Fig. 5C arrows). By 12 weeks of age the R6/2 mice show inclusions in most cells throughout the layers of the cerebellum

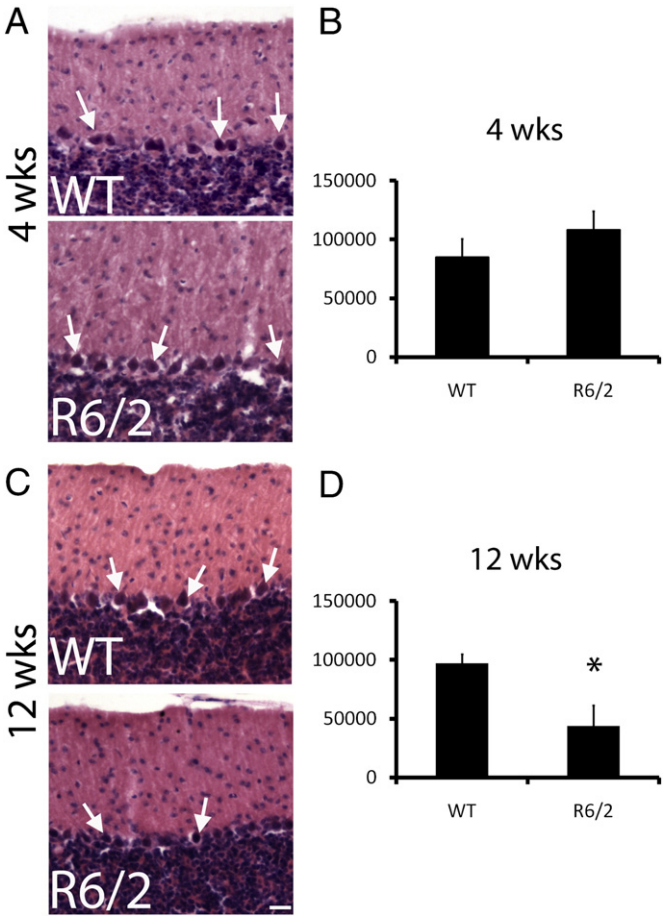

Fig. 3. Cell counts reveal neuronal loss in the Purkinje cell (PC) layer of 12-week-old R6/2 mice. A. Hematoxylin and eosin staining was performed on 30 μm thick cerebellar sections from WT and R6/2 mice. Representative pictures are shown. Staining reveals uniform cell distribution in the cerebellum with no significant differences in stereological counts of PC between WT and R6/2 animals at 4 weeks of age, quantification in B. C. At 12 weeks there is a significant reduction in the number of PCs by 55%, quantification in D. In C, representative pictures are shown of 12-week-old animals. Arrows indicate PCs. n = 3/group. Two-way ANOVA, *$p<0.05$. Error bars represent SEM. Scale bar, 20 μm. n = 3/group at each age tested.

including pronounced inclusions within the PC layer (Fig. 5D, enlarged in Fig. 5F).

Discussion

Huntington Disease is a debilitating neurological disorder. The R6/2 mouse is a severe HD model with an early onset of symptoms and an abbreviated lifespan (Mangiarini et al., 1996). We show that decreases in PC-specific transcript and protein levels occur as part of the disease etiology in the R6/2 mouse model of HD. Furthermore, we demonstrate that PCs are lost during the course of the disease in R6/2 mice and that prior to degeneration- and overt motor symptom onset, PCs are dysfunctional at a physiological level, with a dramatic reduction in firing rate. This demonstration of presymptomatic functional deficits in PCs of R6/2 mice, prior to the appearance of intranuclear inclusions, is novel and suggests that alterations in cerebellar function may contribute to the onset of motor symptoms in this model.

Initial investigations of transcript levels in the cerebellum indicate a loss of the enzyme GAD67 and the calcium-binding proteins PV and Calb by end-stage in the disease time course. Immunohistological staining revealed that these proteins were lost specifically from the PC layer. While a previous report argued for a role in transcriptional downregulations of PV in the cerebellum (Luthi-Carter et al., 2002), the observed loss of PC number associated with transcriptional and protein level changes suggest that these changes are due to a loss of PCs, not transcriptional dysregulation. However, while we did not directly investigate this possibility, reductions in transcript/protein levels in the remaining cells could contribute to alterations in calcium homeostasis and signaling (Llano et al., 1994; Schwaller et al., 2002), which has already been noted in other brain regions in HD (Giacomello et al., 2011; Perry et al., 2010).

Such cell loss occurring in the cerebellum is striking as ataxia is not a common finding in this model (Mangiarini et al., 1996), and PC dysfunction has been shown to cause ataxia-like motor deficits (Walter et al., 2006). While ataxia may not be a key symptom of HD, alterations in gait and balance abnormalities have been observed in both young (5 weeks of age) and end stage mice (Carter et al., 1999; Chiang et al., 2010; Luesse et al., 2001), in addition to symptoms of dystonia (Mangiarini et al., 1996; Stack et al., 2005, 2007). There are also some reports of ataxia and gait disturbances in HD patients (Grimbergen et al., 2008; Koller and Trimble, 1985), although it is possible that more overt manifestations of ataxia are masked by the traditional motor symptoms. Recent work has suggested that disruption of Purkinje cell function by mutations in the α3 isoform of the sodium–potassium ATP-pump causes the dystonia seen in a Dystonia–Parkinsonism mouse model through aberrant interactions with the basal ganglia (Calderon et al., 2011). It is intriguing to postulate that the cerebellum is playing a similar role in the R6/2 model to influence basal ganglia function.

Previously it has been shown that cells of the deep cerebellar nuclei precisely encode spike timing of synchronous PC firing (Person and Raman, 2011). Reductions in GABAergic output from the inhibitory PC could lead to over-excitation in these deep cerebellar nuclei and propagation of misfired cellular signals. Additionally, alterations in spiking patterns could contribute to dysfunctional motor output as the cerebellum forms disynaptic connections with the basal ganglia

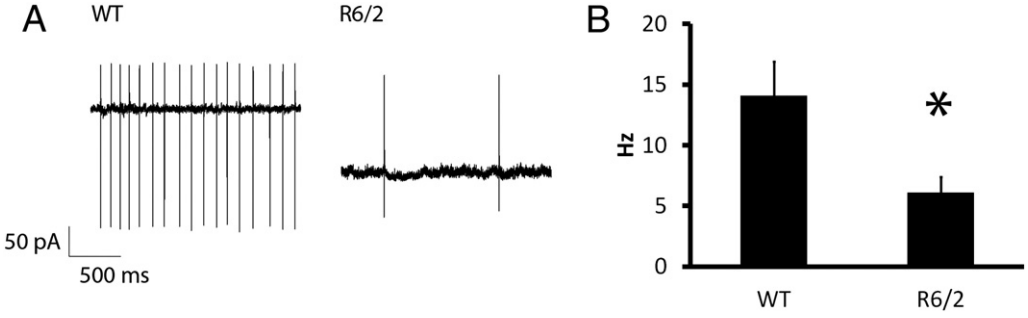

Fig. 4. Purkinje cell spike rate is reduced in presymptomatic R6/2 mice. A. Using presymptomatic R6/2 and age-matched WT mice, loose patch recordings were performed on acute cerebellar slices (300 μm thick); sample traces shown. Recordings lasted for 3 min and were then analyzed using Clampex software; quantification in B. There was a significant difference between event number (spike rate) and inter-event interval (data not shown) between the WT and HD mice (n = 5 and 4 animals for WT and R6/2 respectively; *$p<0.05$). Two-tailed Student's t-tests were performed with error bars representing SEM.

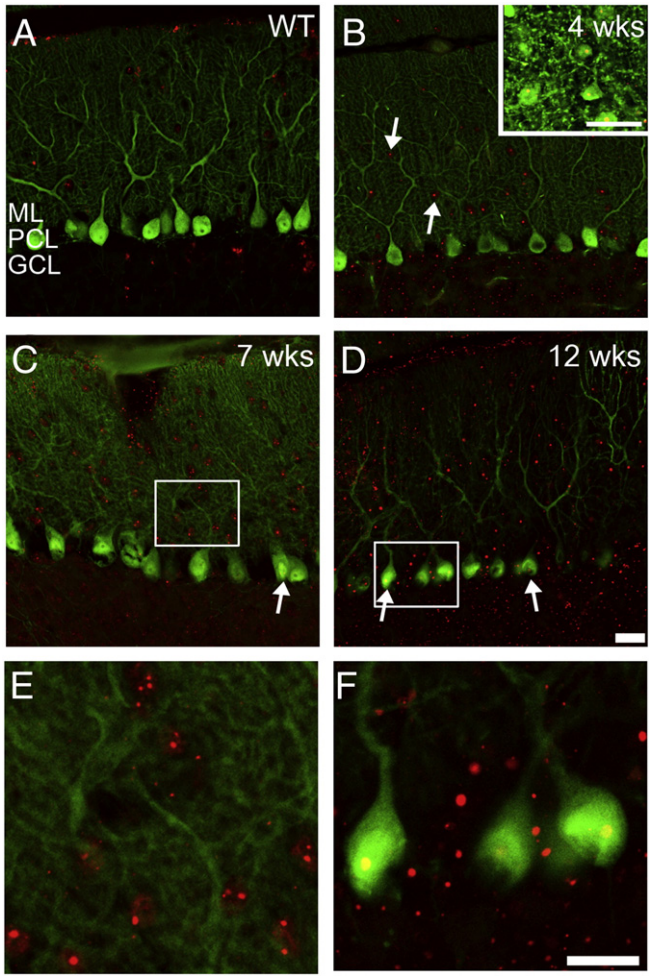

Fig. 5. Huntingtin inclusions are present in the Purkinje cells (PCs) of 12 week R6/2 mice but found in interneurons at a younger age. In order to localize mthtt inclusions to specific cell types in these animals, immunohistochemistry was performed with an antibody specific to mthtt (in red) and calbindin for visualization of the cerebellar layers (in green). In 4-week-old R6/2 animals, mthtt staining is seen in the molecular (arrowheads) and granule cell layers of the cerebellum but not in the PC layer (B). (Inset) Colocalization of the inclusion pathology in 4-week-old R6/2 with parvalbumin (in green) reveals that these aggregates are found within the molecule layer interneurons. Inclusions are absent in 12-week-old WT animals (A). C. 7 week old R6/2 mice exhibit staining throughout the cerebellum, including in a few PC (arrows). Inclusions are seen in the interneurons of the molecular layer, enlarged in E. In 12 week old R6/2 animals, intranuclear inclusions are seen as punctuate staining throughout the PC layer (arrows) and cerebellum (D); representative PCs are highlighted in F ML: molecular layer. PCL: PC layer. GCL: granule cell layer. Scale bar (D), 25 μm. Scale bar (F), 5 μm.

through the thalamus (Bostan and Strick, 2010; Bostan et al., 2010). Interestingly, reports have shown that PC spiking activity is associated with altered levels of GAD67 mRNA (Drengler and Oltmans, 1993; Litwak et al., 1990); it follows that reductions in firing rate could lead to reductions in the mRNA and protein levels that we observed. Further, as PC have been shown to be particularly dependent on activity for survival (Morrison and Mason, 1998), it is possible that a reduction in overall PC activity could contribute to cell death.

To determine what mechanisms could underlie PC loss, we investigated alterations in cellular function and cell-specific accumulation of huntingtin prior to cell loss and the onset of overt motor symptoms. At 4 weeks of age, there was a marked reduction in firing rate in R6/2 mice as compared to the WT. Intriguingly, these firing abnormalities occurred without evidence for huntingtin positive inclusions in PCs. Therefore, the observed reductions in firing rate could reflect cell-autonomous effects of soluble mthtt on membrane properties or, since mthtt staining was readily observed in molecular layer interneurons, non-cell autonomous effects of interneuron dysfunction (Garden et al., 2002). Notably, we observed relative preservation of the molecular layer interneurons, so it is possible that alterations in interneuron function could influence PC firing (increased inhibition). A similar pattern of cell loss (loss of PCs, preservation of interneurons) has been shown previously in a model of spinocerebellar ataxia-1 (Vig et al., 1998). Regarding the toxicity of huntingtin, both soluble and aggregated huntingtin have the potential to be toxic (Lajoie and Snapp, 2010; Weiss et al., 2012); the preservations of the interneurons through the disease time course supports previous reports suggesting the intranuclear inclusions may be protective and not causative in cell death (Arrasate et al., 2004; Kuemmerle et al., 1999).

As previously stated, the R6/2 mouse model is a severe HD mouse model that may more closely replicate a juvenile-onset (JOHD) disease progression (Sawiak et al., 2009). The most severe cases of HD are JOHD and have the longest recorded repeat length. Intriguingly, case studies have shown that JOHD presents not only with the cardinal features of adult onset HD (rigidity, chorea, dementia) but also additional symptoms including a higher occurrence of seizure activity (Hattori et al., 1984; Ruocco et al., 2006a, 2006b). In JOHD, there are multiple reports of cerebellar involvement, atrophy and dysfunction, including fMRI studies showing an incidence of cerebellar atrophy in these most severe patients (Nicolas et al., 2011; Ruocco et al., 2006a, 2006b; Sakazume et al., 2009). Therefore, it is possible that these results may not extend to adult-onset HD mouse models; experiments with HD adult-onset mouse models are required to address this issue.

Our study indicates that the PC population is particularly vulnerable in the R6/2 mouse model. Further experiments are required to determine the extent to which different cell types contribute to PC dysfunction and cell loss, with the goal of designing approaches to rescue this cell population and improve motor function in HD.

Acknowledgments

This work was funded by National Institutes of Health (NIH) Grant 1R01NS070009-01 (R.M.C.). Behavior analysis was conducted in the UAB Evelyn F. McKnight Neurobiology Behavior Core. Imaging studies and stereology were supported by NIH Neuroscience Blueprint Core Grant NS57098 to the University of Alabama at Birmingham. We would also like to acknowledge Dr. David Standaert and his laboratory for microscopy training and access to the Leica confocal microscope.

References

Adachi, H., Kume, A., et al., 2001. Transgenic mice with an expanded CAG repeat controlled by the human AR promoter show polyglutamine nuclear inclusions and neuronal dysfunction without neuronal cell death. Hum. Mol. Genet. 10 (10), 1039–1048.
Arrasate, M., Mitra, S., et al., 2004. Inclusion body formation reduces levels of mutant huntingtin and the risk of neuronal death. Nature 431 (7010), 805–810.
Bithell, A., Johnson, R., et al., 2009. Transcriptional dysregulation of coding and non-coding genes in cellular models of Huntington's disease. Biochem. Soc. Trans. 37 (Pt 6), 1270–1275.
Bostan, A.C., Strick, P.L., 2010. The cerebellum and basal ganglia are interconnected. Neuropsychol. Rev. 20 (3), 261–270.
Bostan, A.C., Dum, R.P., et al., 2010. The basal ganglia communicate with the cerebellum. Proc. Natl. Acad. Sci. U. S. A. 107 (18), 8452–8456.
Calderon, D.P., Fremont, R., et al., 2011. The neural substrates of rapid-onset Dystonia–Parkinsonism. Nat. Neurosci. 14 (3), 357–365.
Carroll, J.B., Lerch, J.P., et al., 2011. Natural history of disease in the YAC128 mouse reveals a discrete signature of pathology in Huntington disease. Neurobiol. Dis. 43 (1), 257–265.
Carter, R.J., Lione, L.A., et al., 1999. Characterization of progressive motor deficits in mice transgenic for the human Huntington's disease mutation. J. Neurosci. 19 (8), 3248–3257.
Cha, J.H., Kosinski, C.M., et al., 1998. Altered brain neurotransmitter receptors in transgenic mice expressing a portion of an abnormal human Huntington disease gene. Proc. Natl. Acad. Sci. U. S. A. 95 (11), 6480–6485.

Chiang, M.C., Chen, C.M., et al., 2010. Modulation of energy deficiency in Huntington's disease via activation of the peroxisome proliferator-activated receptor gamma. Hum. Mol. Genet. 19 (20), 4043–4058.
Cummings, D.M., Andre, V.M., et al., 2009. Alterations in cortical excitation and inhibition in genetic mouse models of Huntington's disease. J. Neurosci. 29 (33), 10371–10386.
Drengler, S.M., Oltmans, G.A., 1993. Rapid increases in cerebellar Purkinje cell glutamic acid decarboxylase (GAD67) mRNA after lesion-induced increases in cell firing. Brain Res. 615 (1), 175–179.
Fennema-Notestine, C., Archibald, S.L., et al., 2004. In vivo evidence of cerebellar atrophy and cerebral white matter loss in Huntington disease. Neurology 63 (6), 989–995.
Garden, G.A., Libby, R.T., et al., 2002. Polyglutamine-expanded ataxin-7 promotes non-cell-autonomous Purkinje cell degeneration and displays proteolytic cleavage in ataxic transgenic mice. J. Neurosci. 22 (12), 4897–4905.
Giacomello, M., Hudec, R., et al., 2011. Huntington's disease, calcium, and mitochondria. Biofactors 37 (3), 206–218.
Grimbergen, Y.A., Knol, M.J., et al., 2008. Falls and gait disturbances in Huntington's disease. Mov. Disord. 23 (7), 970–976.
Group, H. s. D. C. R., 1993. A novel gene containing a trinucleotide repeat that is expanded and unstable on Huntington's disease chromosomes. The Huntington's Disease Collaborative Research Group. Cell 72 (6), 971–983.
Hattori, H., Takao, T., et al., 1984. Cerebellum and brain stem atrophy in a child with Huntington's chorea. Comput. Radiol. 8 (1), 53–56.
Hodges, A., Strand, A.D., et al., 2006. Regional and cellular gene expression changes in human Huntington's disease brain. Hum. Mol. Genet. 15 (6), 965–977.
Imarisio, S., Carmichael, J., et al., 2008. Huntington's disease: from pathology and genetics to potential therapies. Biochem. J. 412 (2), 191–209.
Jeste, D.V., Barban, L., et al., 1984. Reduced Purkinje cell density in Huntington's disease. Exp. Neurol. 85 (1), 78–86.
Kageyama, Y., Yamamoto, S., et al., 2003. A case of adult-onset Huntington disease presenting with spasticity and cerebellar ataxia, mimicking spinocerebellar degeneration. Rinsho Shinkeigaku 43 (1–2), 16–19.
Klapstein, G.J., Fisher, R.S., et al., 2001. Electrophysiological and morphological changes in striatal spiny neurons in R6/2 Huntington's disease transgenic mice. J. Neurophysiol. 86 (6), 2667–2677.
Koeppen, A.H., 1991. The Purkinje cell and its afferents in human hereditary ataxia. J. Neuropathol. Exp. Neurol. 50 (4), 505–514.
Koeppen, A.H., 2005. The pathogenesis of spinocerebellar ataxia. Cerebellum 4 (1), 62–73.
Koller, W.C., Trimble, J., 1985. The gait abnormality of Huntington's disease. Neurology 35 (10), 1450–1454.
Kuemmerle, S., Gutekunst, C.A., et al., 1999. Huntington aggregates may not predict neuronal death in Huntington's disease. Ann. Neurol. 46 (6), 842–849.
Lajoie, P., Snapp, E.L., 2010. Formation and toxicity of soluble polyglutamine oligomers in living cells. PLoS One 5 (12), e15245.
Litwak, J., Mercugliano, M., et al., 1990. Increased glutamic acid decarboxylase (GAD) mRNA and GAD activity in cerebellar Purkinje cells following lesion-induced increases in cell firing. Neurosci. Lett. 116 (1–2), 179–183.
Llano, I., DiPolo, R., et al., 1994. Calcium-induced calcium release in cerebellar Purkinje cells. Neuron 12 (3), 663–673.
Lucas, E.K., Markwardt, S.J., et al., 2010. Parvalbumin deficiency and GABAergic dysfunction in mice lacking PGC-1alpha. J. Neurosci. 30 (21), 7227–7235.
Luesse, H.G., Schiefer, J., et al., 2001. Evaluation of R6/2 HD transgenic mice for therapeutic studies in Huntington's disease: behavioral testing and impact of diabetes mellitus. Behav. Brain Res. 126 (1–2), 185–195.
Luthi-Carter, R., Hanson, S.A., et al., 2002. Dysregulation of gene expression in the R6/2 model of polyglutamine disease: parallel changes in muscle and brain. Hum. Mol. Genet. 11 (17), 1911–1926.
Mangiarini, L., Sathasivam, K., et al., 1996. Exon 1 of the HD gene with an expanded CAG repeat is sufficient to cause a progressive neurological phenotype in transgenic mice. Cell 87 (3), 493–506.
Milnerwood, A.J., Raymond, L.A., 2007. Corticostriatal synaptic function in mouse models of Huntington's disease: early effects of huntingtin repeat length and protein load. J. Physiol. 585 (Pt 3), 817–831.
Morrison, M.E., Mason, C.A., 1998. Granule neuron regulation of Purkinje cell development: striking a balance between neurotrophin and glutamate signaling. J. Neurosci. 18 (10), 3563–3573.
Morton, A.J., Faull, R.L., et al., 2001. Abnormalities in the synaptic vesicle fusion machinery in Huntington's disease. Brain Res. Bull. 56 (2), 111–117.
Nicolas, G., Devys, D., et al., 2011. Juvenile Huntington disease in an 18-month-old boy revealed by global developmental delay and reduced cerebellar volume. Am. J. Med. Genet. A 155A (4), 815–818.
Perry, G.M., Tallaksen-Greene, S., et al., 2010. Mitochondrial calcium uptake capacity as a therapeutic target in the R6/2 mouse model of Huntington's disease. Hum. Mol. Genet. 19 (17), 3354–3371.
Person, A.L., Raman, I.M., 2011. Purkinje neuron synchrony elicits time-locked spiking in the cerebellar nuclei. Nature 481 (7382), 502–505.
Rodda, R.A., 1981. Cerebellar atrophy in Huntington's disease. J. Neurol. Sci. 50 (1), 147–157.
Rosas, H.D., Koroshetz, W.J., et al., 2003. Evidence for more widespread cerebral pathology in early HD: an MRI-based morphometric analysis. Neurology 60 (10), 1615–1620.
Ruocco, H.H., Lopes-Cendes, I., et al., 2006a. Clinical presentation of juvenile Huntington disease. Arq. Neuropsiquiatr. 64 (1), 5–9.
Ruocco, H.H., Lopes-Cendes, I., et al., 2006b. Striatal and extrastriatal atrophy in Huntington's disease and its relationship with length of the CAG repeat. Braz. J. Med. Biol. Res. 39 (8), 1129–1136.
Ruocco, H.H., Bonilha, L., et al., 2008. Longitudinal analysis of regional grey matter loss in Huntington disease: effects of the length of the expanded CAG repeat. J. Neurol. Neurosurg. Psychiatry 79 (2), 130–135.
Sakazume, S., Yoshinari, S., et al., 2009. A patient with early onset Huntington disease and severe cerebellar atrophy. Am. J. Med. Genet. A 149A (4), 598–601.
Sawiak, S.J., Wood, N.I., et al., 2009. Voxel-based morphometry in the R6/2 transgenic mouse reveals differences between genotypes not seen with manual 2D morphometry. Neurobiol. Dis. 33 (1), 20–27.
Schulz, J.B., Borkert, J., et al., 2010. Visualization, quantification and correlation of brain atrophy with clinical symptoms in spinocerebellar ataxia types 1, 3 and 6. Neuroimage 49 (1), 158–168.
Schwaller, B., Meyer, M., et al., 2002. 'New' functions for 'old' proteins: the role of the calcium-binding proteins calbindin D-28k, calretinin and parvalbumin, in cerebellar physiology. Studies with knockout mice. Cerebellum 1 (4), 241–258.
Stack, E.C., Kubilus, J.K., et al., 2005. Chronology of behavioral symptoms and neuropathological sequela in R6/2 Huntington's disease transgenic mice. J. Comp. Neurol. 490 (4), 354–370.
Stack, E.C., Dedeoglu, A., et al., 2007. Neuroprotective effects of synaptic modulation in Huntington's disease R6/2 mice. J. Neurosci. 27 (47), 12908–12915.
Strand, A.D., Aragaki, A.K., et al., 2005. Gene expression in Huntington's disease skeletal muscle: a potential biomarker. Hum. Mol. Genet. 14 (13), 1863–1876.
Van Raamsdonk, J.M., Warby, S.C., et al., 2007. Selective degeneration in YAC mouse models of Huntington disease. Brain Res. Bull. 72 (2–3), 124–131.
Vig, P.J., Fratkin, J.D., et al., 1996. Decreased parvalbumin immunoreactivity in surviving Purkinje cells of patients with spinocerebellar ataxia-1. Neurology 47 (1), 249–253.
Vig, P.J., Subramony, S.H., et al., 1998. Reduced immunoreactivity to calcium-binding proteins in Purkinje cells precedes onset of ataxia in spinocerebellar ataxia-1 transgenic mice. Neurology 50 (1), 106–113.
Walter, J.T., Alvina, K., et al., 2006. Decreases in the precision of Purkinje cell pacemaking cause cerebellar dysfunction and ataxia. Nat. Neurosci. 9 (3), 389–397.
Weiss, K.R., Kimura, Y., et al., 2012. Huntingtin aggregation kinetics and their pathological role in a *Drosophila* Huntington's disease model. Genetics 190 (2), 581–600.